Chemistry & Biology
Article

Structural and Mechanistic Insights into C-P Bond Hydrolysis by Phosphonoacetate Hydrolase

Vinayak Agarwal,[1,5] Svetlana A. Borisova,[5,6] William W. Metcalf,[4,5] Wilfred A. van der Donk,[2,3,5,6,*] and Satish K. Nair[1,2,5,*]
[1]Center for Biophysics and Computational Biology
[2]Department of Biochemistry
[3]Department of Chemistry
[4]Department of Microbiology
[5]Institute for Genomic Biology
[6]Howard Hughes Medical Institute
University of Illinois at Urbana-Champaign, Urbana, IL 61801, USA
*Correspondence: vddonk@illinois.edu (W.A.v.d.D.), s-nair@life.illinois.edu (S.K.N.)
DOI 10.1016/j.chembiol.2011.07.019

SUMMARY

Bacteria have evolved pathways to metabolize phosphonates as a nutrient source for phosphorus. In *Sinorhizobium meliloti* 1021, 2-aminoethylphosphonate is catabolized to phosphonoacetate, which is converted to acetate and inorganic phosphate by phosphonoacetate hydrolase (PhnA). Here we present detailed biochemical and structural characterization of PhnA that provides insights into the mechanism of C-P bond cleavage. The 1.35 Å resolution crystal structure reveals a catalytic core similar to those of alkaline phosphatases and nucleotide pyrophosphatases but with notable differences, such as a longer metal-metal distance. Detailed structure-guided analysis of active site residues and four additional cocrystal structures with phosphonoacetate substrate, acetate, phosphonoformate inhibitor, and a covalently bound transition state mimic provide insight into active site features that may facilitate cleavage of the C-P bond. These studies expand upon the array of reactions that can be catalyzed by enzymes of the alkaline phosphatase superfamily.

INTRODUCTION

Phosphonic and phosphinic acids contain a stable carbon-phosphorus (C-P) bond in place of the oxygen-phosphorus (O-P) bonds found in phosphate esters (Metcalf and van der Donk, 2009). These compounds are ubiquitous in biological systems, as exemplified by their occurrence in lipids, exopolysaccharides, and glycoproteins. The structural resemblance of several small molecule phosphonates to the corresponding phosphoric acid esters and anhydrides renders these phosphonates competitive inhibitors of enzymatic processes involved in phosphoryl transfer reactions. Phosphonates with biological activities include antifungals (rhizocticin), herbicides (glyphosate and phosphinothricin tripeptide [PTT]), antibacterials (dehydrophos and fosfomycin), and antimalarials (fosmidomycin and FR900098) (Figure 1A).

A characterization of marine dissolved organic matter estimates that phosphonic acids constitute nearly one quarter of the available phosphorus in the world's oceans, and, in some organisms, phosphonates represent the most abundant of sources of phosphorus (Clark et al., 1999). Given this prevalence, it is not surprising that several microorganisms have evolved pathways for the degradation of phosphonates for use as sources of carbon and phosphorus (Quinn et al., 2007; White and Metcalf, 2007). Thus far, four different enzyme activities that cleave C-P bonds have been identified, and these can be divided into two mechanistic classes (Kononova and Nesmeyanova, 2002). The first class consists of carbon-phosphorus lyases, membrane-associated multienzyme systems that can directly cleave unactivated C-P bonds of several structurally diverse substrates, presumably using redox chemistry (Wackett et al., 1987). The second class consists of enzymes acting on phosphonates that contain an electron-withdrawing β-carbonyl group and includes phosphonopyruvate (PnPy) hydrolase, phosphonoacetaldehyde (PnAA) hydrolase, and phosphonoacetate (PnA) hydrolase (Figure 1B). Phosphonopyruvate hydrolase acts on PnPy that is reversibly generated from either phosphonoalanine by PnPy transaminase or from phosphoenolpyruvate (PEP) by PEP phosphomutase (Chen et al., 2006). Phosphonoacetaldehyde hydrolase hydrolyzes PnAA that is produced from phosphonopyruvate by PnPy decarboxylase (Morais et al., 2000). Phosphonoacetate hydrolase cleaves PnA to yield acetate and inorganic phosphate (Pi) (McGrath et al., 1995).

Although the biogenic origin of PnA has only recently gained some experimental support (Panas et al., 2006), PnA hydrolysis activity was observed in the crude extracts of *Pseudomonas fluorescens* 23F (McMullan et al., 1992). The enzyme was purified from the native producer and was shown in vitro to catalyze the zinc-dependent hydrolysis of PnA (McGrath et al., 1995). Subsequently, the corresponding gene (designated *phnA*) was cloned and the gene product was heterologously produced in bacteria (Kulakova et al., 1997). PnA hydrolysis activity has since been demonstrated in other *Pseudomonas* species (Panas et al., 2006), *Penicillium* species (Forlani et al., 2006), marine bacteria, and coral holobionts (Thomas et al., 2010), establishing the presence of PhnA-mediated PnA hydrolysis in the microbial metabolome.

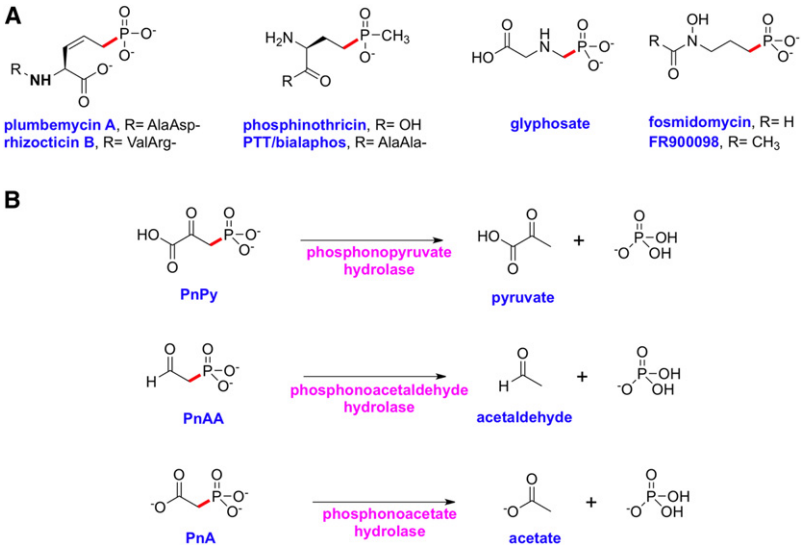

Figure 1. Chemical Structures of Representative Phosphonates and Enzyme Activities that Result in the Cleavage of C-P Bonds

(A) Chemical structures of phosphonates with demonstrated biological activity.

(B) Enzymatic cleavage of C-P bonds in phosphonate substrates containing an electron-withdrawing β-carbonyl group.

Primary sequence analysis reveals PhnA to be a member of the alkaline phosphatase (AP) superfamily (Coleman, 1992; Galperin et al., 1998; Kulakova et al., 1997). Alkaline phosphatases and the related nucleotide pyrophosphatases/phosphodiesterases (NPPs) catalyze the hydrolysis of phosphate monoesters and diesters, respectively. The active site of these enzymes consists of a binuclear metal core and contains a catalytically required Ser or Thr that generates a covalent phosphoenzyme intermediate (Holtz et al., 1999). Alkaline phosphatases from disparate sources differ in the identity of the divalent metal ions in the active site (Wojciechowski et al., 2002). The metal ion specificity is rendered in part by the identity of the active site residues and can be changed by mutagenesis of the metal-coordinating amino acid side chains (Wang et al., 2005; Wojciechowski and Kantrowitz, 2002).

Compared to the extensive investigations into the mechanism and substrate specificity of phosphate monoester and diester hydrolysis, the hydrolysis of phosphonates is a much less studied activity within the catalytic repertoire of the alkaline phosphatase superfamily. The mechanism by which a member of the AP superfamily catalyzes this process is of great interest given the very different, carbon-based leaving group in C-P bond hydrolysis. In order to elucidate the mechanistic basis for C-P (rather than O-P) bond hydrolysis, we present detailed kinetic and structural studies of PhnA from *Sinorhizobium meliloti* 1021. Crystal structures of the wild-type enzyme confirm structural similarity to alkaline phosphatases but with notable differences that likely direct activity toward the cleavage of a C-P bond. Kinetic analyses of metal-substituted PhnA and corresponding anomalous scattering diffraction experiments on zinc- and manganese-containing PhnA establish the in vitro metal preference. Cocrystal structures with substrate PnA, product acetate ion, inhibitor phosphonoformate (PnF), and the transition state mimic vanadate, together with kinetic and structural analysis of site-specific active site variants, suggest a plausible mechanism for PnA hydrolysis by PhnA. Our results expand upon a very recent study of a PnA hydrolase from *P. fluorescens* 23F (Kim et al., 2011).

RESULTS

Overall Structure

The PhnA protein from *S. meliloti* was heterologously produced in *Escherichia coli* with an amino-terminal hexahistidine tag. For crystallization, the tag was removed via thrombin protease cleavage. Initial crystallographic phases for the wild-type PhnA were determined by single-wavelength anomalous diffraction data collected on crystals grown from selenomethionine-labeled protein, and the structure has been subsequently refined to 1.35 Å resolution to a free R value of 21%. Relevant data collection and refinement statistics are provided in Table 1. The overall structure of PhnA is shown in Figure 2A.

The structure of PhnA consists of two distinct domains: a core domain that is highly homologous within members of the alkaline phosphatase superfamily (Figures 2B and 2C) and a divergent capping domain that has only previously been observed in the structure of NPP from *Xanthomonas axonopodis pv. citri* (Figure 2C) (Zalatan et al., 2006) and, very recently, in the crystal structure of PnA hydrolase from *P. fluorescens* 23F (Kim et al., 2011). The core domain comprises residues Met4-Gly85, Asp104-Met253, and Ser376-Ala416 and consists of a seven-membered β sheet flanked by eight α helices on either side. The capping domain has a typical α/β/α fold and is composed of residues Lys254-Arg375. Of particular note is the β-loop-β appendage comprising of residues Ile86-Asn103, which extends from the helices of the core domain and contacts the central β sheet of the capping domain (Figure 2A). This appendage is also present in the crystal structure of NPP (Zalatan et al., 2006) (Figure 2C) but is absent in the structures of alkaline phosphatases that hydrolyze phosphate monoesters (Figure 2B). The structures described here are more complete and of higher resolution than the previously reported structure of *P. fluorescens* 23F PnA hydrolase (PDB ID: 1EI6) (Kim et al., 2011), in which several residues proximal to the active site were disordered and consequently were not modeled. The current structure presents complete modeling of all residues of the β-loop-β appendage and all surface loops of the core domain.

Active Site Metal Ions

Members of the alkaline phosphatase superfamily are characterized by the presence of two requisite metal ions, and the nature of the metal-coordinating protein ligands is highly conserved (Coleman, 1992). Likewise, PhnA contains two metal ions (referred to as M1 and M2, consistent with nomenclature for this superfamily), with M1 coordinated by His215, His377, and

Table 1. Data Collection, Phasing, and Refinement Statistics

	PhnA (native)	PhnA-Vanadate	T68A PhnA-PnA	PhnA-Acetate	PhnA-PnF
Data Collection					
Space group	$P4_32_12$	$P4_32_12$	$P4_32_12$	$P4_32_12$	$P4_32_12$
Cell dimensions					
a, b, c (Å)	111.8, 111.8, 72.8	111.1, 111.1, 72.4	111.4, 111.4, 72.8	111.4, 111.4, 72.9	111.6, 111.6, 72.5
Resolution (Å)[a]	50–1.35 (1.4–1.35)	50–1.8 (1.83–1.8)	40–2.0 (2.07–2.0)	50–2.0 (2.03–2.0)	50–1.6 (1.66–1.6)
R_{sym} (%)	6.8 (60.8)	6.5 (69.3)	7.5 (47.4)	7.1 (16.9)	8.0 (38.0)
I / σ (I)	36.8 (1.7)	36.2 (2.2)	32.1 (2.5)	47.5 (5.5)	33.0 (3.9)
Completeness (%)	98.3 (84.6)	98.0 (91.6)	99.4 (94.3)	100.0 (99.9)	99.3 (96.4)
Redundancy	10.4 (4.0)	10.9 (7.8)	11.2 (5.5)	11.3 (10.9)	11.3 (9.0)
Refinement					
Resolution (Å)	25.0–1.35	25.0–1.8	25.0–2.0	25.0–2.0	25.0–1.6
No. of reflections	94,012	39,623	29,711	29,946	57,337
R_{work} / R_{free}[b]	19.7/20.9	20.5/24.1	18.9/23.4	17.6/21.9	19.3/21.6
No. of atoms					
Protein	3204	3194	3192	3199	3200
Metal	2	2	2	2	2
Ligand	-	5	8	4	7
Water	583	351	280	379	565
B-factors					
Protein	13.8	28.3	32.2	17.2	15.8
Metal	19.3	32.4	25.6	45.4	13.8
Ligand	-	31.8	36.8	25.6	21.5
Water	28.5	34.7	36.1	28.2	20.0
Rms deviations					
Bond lengths (Å)	0.006	0.007	0.010	0.009	0.006
Bond angles (°)	1.06	1.05	1.19	1.12	1.08

[a] Highest resolution shell is shown in parentheses.
[b] R-factor = $\Sigma(|F_{obs}|-k|F_{calc}|)/\Sigma |F_{obs}|$ and R-free is the R value for a test set of reflections consisting of a random 5% of the diffraction data not used in refinement.

Asp211 and M2 coordinated by Asp29, Asp250, and His251 (Figure 3A; see Figure S1A, available online). As in other members of the alkaline phosphatase superfamily, metal M2 likely activates the catalytic Thr68 for nucleophilic attack at the phosphorus atom (Kim et al., 2011; Schwartz and Lipmann, 1961), and metal M1 likely activates a water molecule for nucleophilic displacement at the phosphorus atom during hydrolysis of the phosphorylated enzyme intermediate (Coleman, 1992). The two metal ions also contribute to electrostatic stabilization of the negative charge on the nonbridging oxygens during catalysis of P-O bond cleavage (Lassila and Herschlag, 2008; Nikolic-Hughes et al., 2005).

The bound metal ions in PhnA (as purified from heterologous overexpression in *E. coli*) are zinc ions; their identity and location were determined using anomalous diffraction data collected at the zinc absorption edge (Figure 3A). Interestingly, the distance between the two metal ions was 4.60 Å. This distance is significantly greater than the distance between the metal ions in *E. coli* AP (4.26–4.28 Å; PDB ID: 1ED9) (Figure 3B) and NPP (4.26–4.36 Å; PDB ID: 2GSN) (Figure 3C), and to the best of our knowledge is greater than the distance reported for any other alkaline phosphatase superfamily members (Stec et al., 2000; Zalatan et al., 2006). A similarly long metal-metal distance was also reported for the PnA hydrolase from *P. fluorescens* (4.47 Å) (Kim et al., 2011).

In alkaline phosphatases, a third metal (typically magnesium) is located in the active site and was postulated to be critical for deprotonation of the serine side chain to generate the alkoxide nucleophile (Kim and Wyckoff, 1991). This third metal is absent in PhnA, as has also been observed in the structure of NPP (Zalatan et al., 2006). Absence of the third metal ion in NPP has led to re-evaluation of its role in phosphoryl group transfer reactions mediated by alkaline phosphatases. More recent studies comparing the reactivities of monoester and diester substrates suggest that the magnesium ion stabilizes a nonbridging oxygen atom in the transition state for phosphate monoester hydrolysis (Zalatan et al., 2008). In the PhnA structure, side chains of residues Cys27, Asp29, Asn72, Tyr206, and Thr208 form a hydrogen-bonding network replacing the region corresponding to the third metal site in alkaline phosphatases. The mechanistic implications of the absence of this third metal in the structure of PhnA are not immediately clear.

Metal Ion Specificity

Alkaline phosphatases can utilize a vast array of divalent metal ions in the catalytic M1 and M2 positions, with the metal ion

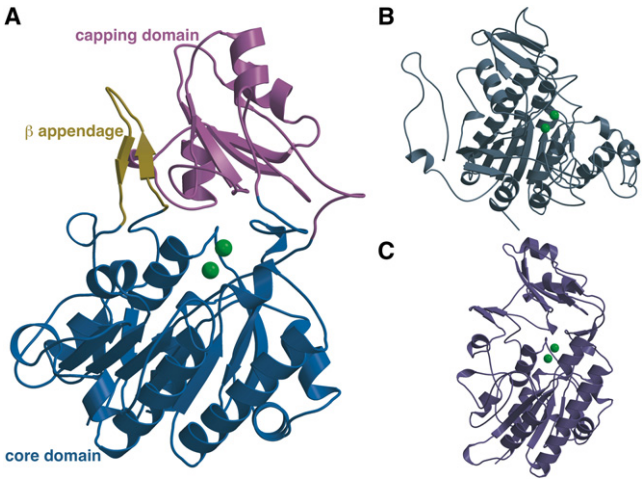

Figure 2. Overall Structure of PhnA as Compared to Structures of AP and NPP

(A) Structure of PhnA showing the core catalytic domain that is conserved among members of the AP superfamily (blue) and the β appendage (yellow) and capping domain (pink) that are specific to PhnA and NPP. The two metal ions are shown as green spheres.

(B) Structure of *E. coli* AP (PDB Code: 1B8J).

(C) Structure of *X. axonopodis* NPP (PDB Code: 2GSO).

specificity subject to change by alterations in the active site amino acid side chains (Wojciechowski and Kantrowitz, 2002). To probe the specific metal ion preference for PhnA, we monitored the catalytic efficiency of the enzyme that was overexpressed and purified from *E. coli* and after its incubation with Mg^{2+}, Zn^{2+}, Co^{2+}, Fe^{2+}, and Mn^{2+} (Table 2; Figure S2). As previously reported (Borisova et al., 2011), the enzyme purified from *E. coli* efficiently catalyzed the hydrolysis of PnA without the addition of metal ions. When PhnA was incubated with Zn^{2+} prior to the activity assay, a small improvement in k_{cat} was observed along with an increase in K_M. However, when PhnA was preincubated with Mn^{2+} or Fe^{2+}, 2–3-fold improvement in k_{cat} was observed with only small variations in the K_M values (Table 2). Activity assays in the presence of Mg^{2+} or Co^{2+} resulted in decreased k_{cat} values, with a substantially lower K_M value of PhnA reconstituted with Co^{2+} compensating for the lower turnover number of this enzyme.

Enzyme purified from *E. coli* was treated with the metal ion chelator ethylenediamine tetraacetic acid (EDTA) to remove the metal ions already bound to the enzyme. The resulting apo-PhnA was devoid of enzymatic activity. However, the activity was fully reconstituted by brief incubation of PhnA with different divalent metal ions prior to the activity assays (Table 2; Figure S2). Thus, the addition of Zn^{2+} produced a form of PhnA with kinetic parameters nearly identical to those of the as-isolated enzyme. The greatest increase in the enzymatic activity was observed upon reconstitution of EDTA-treated PhnA with Mn^{2+}, resulting in a k_{cat}/K_M value 4-fold higher than that found for as-isolated PhnA. When combinations of equal concentrations of either Fe^{2+} and Zn^{2+} or Mn^{2+} and Zn^{2+} were tested for apo-PhnA reconstitution, the activity of the enzyme did not exceed that of Zn-reconstituted PhnA (Table S1), suggesting that it is present predominantly as the Zn-bound form in either preparation and that PhnA has the greatest affinity for Zn^{2+}. The identity of the PhnA-bound metal ion(s) in PhnA reconstituted with different metals could not be characterized directly because of partial dissociation of the bound metal ions from PhnA during attempts to separate the protein from the constituents of the reconstitution buffer.

In order to probe whether differences in activity were a consequence of structural changes between the zinc- and manganese-substituted enzymes, we collected anomalous diffraction data on Mn^{2+}-substituted PhnA. Double difference Fourier maps were calculated, which showed unambiguous positive density for metal ions in the M1 and M2 positions only at the manganese absorption edge, ensuring that both sites of the recombinant PhnA were occupied by manganese under the conditions used. The structure of Mn^{2+}-PhnA is virtually identical to that of Zn^{2+}-PhnA, including the metal-metal distance (4.6 Å), suggesting that the structural results detailed below are valid

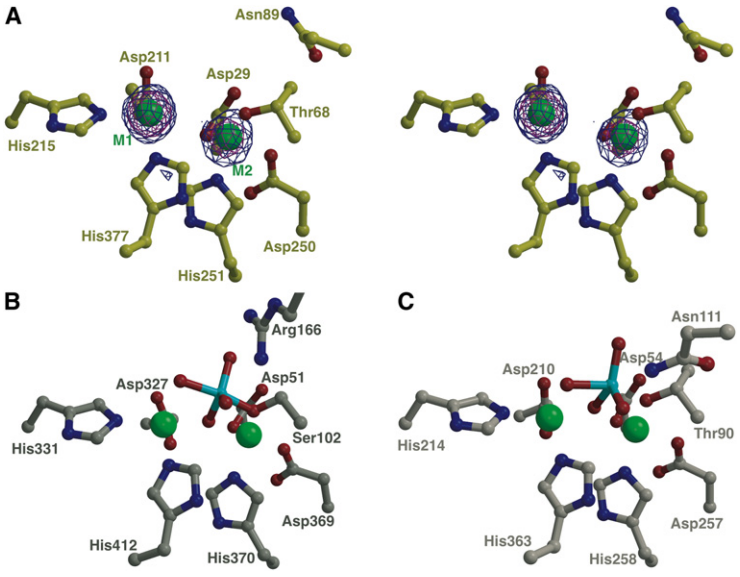

Figure 3. Active Site View of PhnA as Compared to AP and NPP

(A) Stereo view of PhnA active site showing a Bijvoet difference map, calculated using Fourier coefficients |F(+)| and |F(-)| from data collected at the zinc absorption edge and phases from the final refined model without any metal ions. The map is contoured at 3σ (in blue) and 10σ (in red). The coordinates from the final refined model are superimposed and the two metal ions are shown as green spheres.

(B and C) The active site view of *E. coli* AP (PDB Code: 1B8J) (B) and of *X. axonopodis* NPP (PDB Code: 2GSO) (C), both in complex with the inhibitor vanadate (colored in cyan), are shown for comparison. Water molecules are omitted for clarity. See also Figure S1A.

Table 2. Kinetic Parameters for PnA Hydrolysis by PhnA in the Presence of Different Metal Ions (10 μM)

PhnA-N-His	k_{cat}, s^{-1}	K_M, μM	k_{cat}/K_M, $M^{-1}s^{-1}$	k_{cat}/K_M, rel.
As isolated[a]	0.91 ± 0.03	22 ± 2	4.1×10^4	1
+ Zn^{2+a}	1.06 ± 0.02	37 ± 2	2.9×10^4	0.7
+ Fe^{2+}	3.6 ± 0.1	43 ± 5	8.4×10^4	2.0
+ Mn^{2+}	2.60 ± 0.07	34 ± 3	7.7×10^4	1.9
+ Co^{2+}	0.57 ± 0.02	11 ± 2	5.1×10^4	1.2
+ Mg^{2+}	0.18 ± 0.01	34 ± 5	0.5×10^4	0.1
Apo PhnA	No activity detected			
+ Mn^{2+}	5.5 ± 0.2	34 ± 3	16.2×10^4	4.0
+ Fe^{2+}	3.6 ± 0.2	44 ± 8	8.0×10^4	2.0
+ Zn^{2+}	1.16 ± 0.03	30 ± 3	3.8×10^4	0.9

See also Table S1.
[a] Reported in Borisova et al. (2011).

for enzyme containing either metal. It should be noted that the values of kinetic constants observed for any of the metal-bound forms of PhnA (Table 2) are within the physiologically relevant range. Thus, it is possible that the identity of the PhnA-bound metal in vivo is determined not only by the affinity of the PhnA metal-binding sites but also by the intracellular levels of metal ions in *S. meliloti*, which have not been reported to date.

Model for a Transition State Structure

Hydrolysis of phosphate esters by alkaline phosphatases takes place by an in-line double displacement mechanism in which the alkoxide ion, generated on a serine or threonine side chain, first attacks the tetracoordinated phosphorus atom. This displacement of a metal-stabilized leaving group by the enzyme nucleophile occurs via a trigonal bipyramidal transition state, leading to the formation of a covalent phosphoseryl (or phosphothreonyl) intermediate (Coleman, 1992). Hydrolysis of this intermediate involves the attack of a M1-bound hydroxide onto the phosphorus atom displacing the Ser/Thr via another trigonal bipyramidal transition state. The covalent adduct of orthovanadate ion with the catalytic serine or threonine side chain mimics the trigonal bipyramidal geometry of the transition state with the nucleophile and the leaving group occupying the axial positions; three of the oxygen atoms attached to the vanadium atom occupy the equatorial positions. Complexes with vanadate have been reported for both AP and NPP, have led to insights into the stabilization of the reaction transition state (Holtz et al., 1999; Zalatan et al., 2006), and have facilitated the identification of stabilizing interactions for each of the equatorial oxygen atoms. For both enzymes, one oxygen atom is directed in between the metal ions and is stabilized by electrostatic interactions. Two other equatorial oxygen atoms in *E. coli* AP are stabilized by interactions with the guanidinium group of Arg166. For NPP, in which phosphate diester hydrolysis results in two, instead of three, nonbridging equatorial oxygen atoms, Asn111 (in *X. axonopodis*) interacts with one of these oxygen atoms to stabilize the transition state.

In order to delineate the interactions that occur in the transition state for phosphonate C-P bond hydrolysis by PhnA, we have determined the cocrystal structure of a covalent complex with orthovanadate at 1.65 Å resolution (Figure 4A). As observed for NPP (Zalatan et al., 2006) and AP (Holtz et al., 1999), the trigonal bipyramidal structure of the orthovanadate adduct is slightly distorted, with the O-V-O bond angle for the axial oxygens being 168° in PhnA compared to 157° for NPP and 170° for AP. Unlike AP and NPP, the three equatorial oxygens are not in a plane with the vanadate atom but are tilted toward the M2 ion (Figure 4A). A decrease in the distance between the two zinc ions of 0.3 Å is observed compared to the structure of unliganded PhnA. The side chain hydroxyl of Thr68 is placed in one of the axial positions, and the oxygen atom at the other axial position interacts with the zinc ion in the M1 site, which corresponds to the leaving group stabilization by the metal ion in a phosphate ester hydrolysis reaction. One of the equatorial oxygen atoms is situated in between the zinc atoms at a distance of 1.8 Å to M2 and a longer distance of 2.6 Å to M1, whereas a second equatorial oxygen is within hydrogen bonding distance (2.7 Å) of the amide bond nitrogen of Thr68 (Figure S1B). However, unlike NPP, where an additional hydrogen bond from the side chain of Asn111 further stabilizes the equatorial oxygen, no appropriately placed amino acid side chains are within hydrogen bonding distance. The strictly conserved Asn89, corresponding to Asn111 of NPP, is too distant (5.46–5.65 Å) to be involved in a direct contact. A water molecule coordinated by the side chain of Asn89 is placed 3.5 Å away from this equatorial oxygen and this water molecule additionally interacts with the backbone nitrogen of Asn69 (Figure S1B). When Asn89 was replaced with valine, the catalytic activity of the PhnA-N89V mutant was reduced by approximately 10^4-fold as compared to the wild-type PhnA (Table S1). A crystal structure of the N89V mutant determined at 1.8 Å resolution revealed that both metal ions are preserved in the mutant structure and that no major rearrangements of the amino acid side chains around the active site could be observed. However, the arrangement of the water molecules in the active site is different from that of the wild-type enzyme (data not shown), supporting the contribution of the water-mediated contact to the Asn89 side chain to transition state stabilization. In AP, the third equatorial oxygen atom is hydrogen bonded to Arg166; in NPP, this oxygen carries a substituent in the phosphodiester substrate and does not have any interaction partners in the NPP crystal structure. In PhnA, this third oxygen makes water-mediated contacts in the PhnA-vanadate structure (Figure S1B). A water molecule, hydrogen bonded to the carboxylate side chain of Asp29, is positioned 3.2 Å away.

Crystal Structure of PhnA with Acetate Bound

Diffraction data from crystals of wild-type PhnA soaked with PnA reveal the appearance of electron density consistent with an acetate ion bound to the M1 metal ion (Figure 4B; Figure S1C). Two lines of evidence suggest that the resultant electron density for acetate derives from turnover of the PnA substrate by PhnA: first, diffraction data from crystals grown under identical conditions but without the addition of PnA do not show density for acetate; second, no contamination of acetate could be detected in samples of PnA used for cocrystallization as determined by proton NMR spectroscopy.

In the 2.0 Å resolution PhnA-acetate cocrystal structure, both oxygen atoms of the acetate ion are coordinating to the M1 metal ion at a distance of 2.1 Å (Figure 4B). Coordination of the two

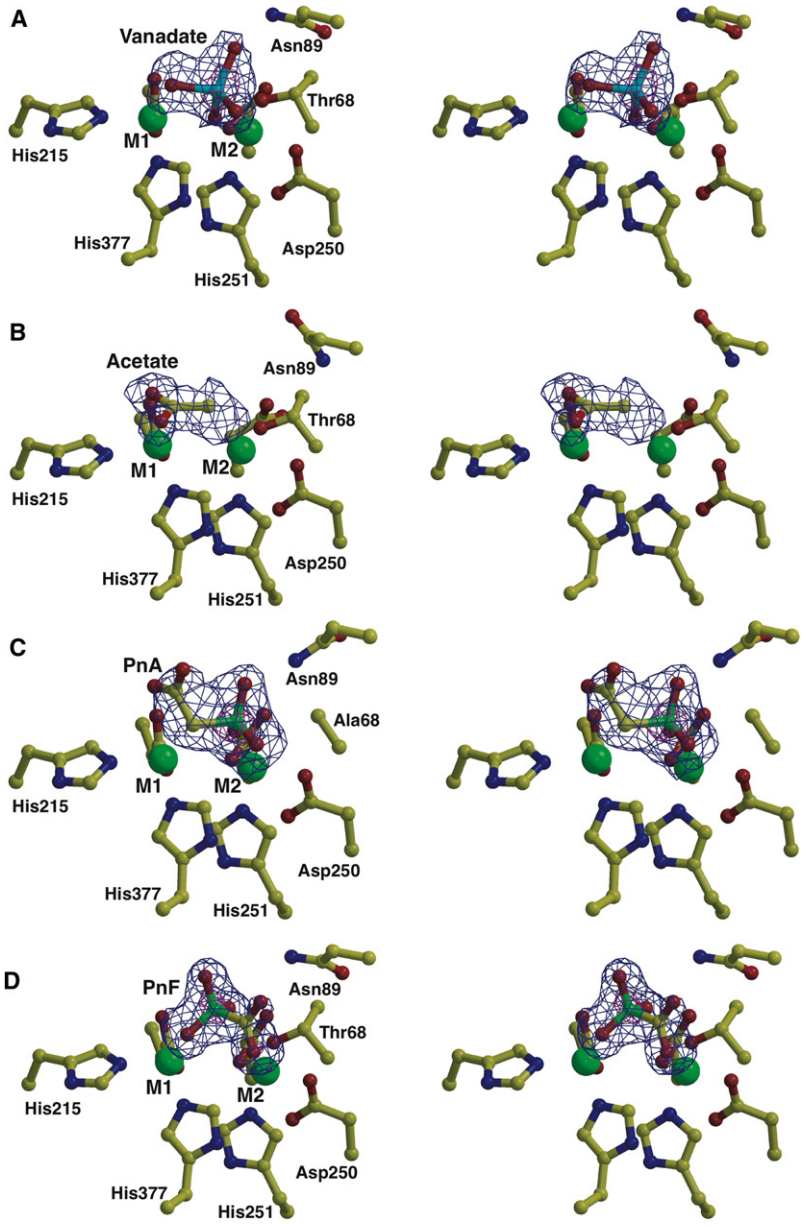

Figure 4. Stereo Views of PhnA Active Site with Ligands Bound

(A) Stereo view showing the active site features of the PhnA-vanadate structure. The vanadate is colored in cyan, polypeptide residues are shown in yellow, and the active site metals are shown as green spheres. Superimposed is a difference Fourier electron density map (contoured at 3σ over background in blue and 8σ over background in pink) calculated with coefficients $|F_{obs}| - |F_{calc}|$ and phases from the final refined model with the coordinates of vanadate deleted prior to one round of refinement.

(B) Stereo view of the active site features of the PhnA-acetate complex. Residues are colored as above and superimposed is a difference Fourier electron density map (contoured at 3σ over background in blue) calculated with coefficients $|F_{obs}| - |F_{calc}|$ and phases from the final refined model with the coordinates of acetate deleted prior to one round of refinement.

(C) Stereo view of the active site features of the PhnA-T68A-PnA complex. Residues are colored as above and superimposed is a difference Fourier electron density map (contoured at 3.3σ over background in blue and 10σ over background in pink) calculated with coefficients $|F_{obs}| - |F_{calc}|$ and phases from the final refined model with the coordinates of PnA deleted prior to one round of refinement.

(D) Stereo view of the active site features of the PhnA-PnF complex. Residues are colored as above and superimposed is a difference Fourier electron density map (contoured at 3σ over background in blue and 8σ over background in pink) calculated with coefficients $|F_{obs}| - |F_{calc}|$ and phases from the final refined model with the coordinates of PnF deleted prior to one round of refinement. In all panels, water molecules are omitted for clarity. See also Figures S1 and S3.

oxygen atoms of the carboxylate moiety of acetate by the M1 metal ion places the methyl group of acetate 2.4 Å from the M1 metal ion and 3.9 Å from the M2 metal ion. Although not observed in the structure, the spacing between the acetate and M2 metal ion is sufficient to accommodate a phosphate group covalently bound to Thr68. One water molecule is positioned 2.85 Å away from the methyl group of the acetate and is stabilized by hydrogen bond interactions with the backbone carbonyl of Ile287 and backbone amide nitrogen of Asn69 (Figure S1C).

Cocrystal Structure of PhnA-T68A with Phosphonoacetate

Attempts at cocrystallization of wild-type PhnA enzyme, or soaking of apo wild-type enzyme crystals with substrate PnA, were unsuccessful because, across all concentrations of substrate employed, catalytic turnover of the substrate lead to incorporation of the acetate ion in the active site of the enzyme, and no density of the phosphate moiety could be observed. Hence cocrystallization of PnA with a T68A mutant (exhibiting an approximately 10^3-fold decrease in activity; Table S1) was attempted. Crystals for the T68A mutant showed robust density for PnA in the active site (Figure 4C; Figure S1D). The identity of the ligand is affirmed by the presence of strong electron density at a position corresponding to the electron-dense phosphorus atom of the substrate. The phosphonate group of the substrate molecule is bound in a manner consistent with the transition state model predicted by the vanadate covalent crystal structure. The phosphorus atom is 3.4 Å away from the side chain methyl group of alanine at position 68 (corresponding to the position of the Thr nucleophile). One oxygen atom of the phosphonate of PnA points toward the M2 metal ion and is positioned at a distance of 1.99 Å. A second oxygen atom is hydrogen bonded to the backbone amide of Ala68, 2.69 Å from the amide nitrogen. This oxygen also engages in a water-mediated contact with the side chain of Asn69. A water-mediated hydrogen bond also exists between Asp29 and the third phosphonate oxygen atom (Figure S1D).

Superposition of the apo wild-type PhnA structure onto the PhnA-T68A-PnA structure positions the catalytic threonine side chain hydroxyl 1.8 Å from the phosphorus atom, and the theoretical bond angle between the hydroxyl oxygen, phosphorus atom, and methylene group of PnA is 163°, close to the 168° seen for the vanadate transition state mimic. For comparison, the bond length between the vanadate atom and the catalytic threonine hydroxyl oxygen in the covalent complex is 2.0 Å. Thus, the position of the phosphonate group in the T68A mutant is slightly skewed toward the threonine hydroxyl as compared to the vanadate transition state model.

The acetate moiety of the substrate is bound in a different manner to the T68A mutant compared to the acetate-bound state of the wild-type enzyme described above. Although the acetate ion binds to the M1 metal ion in a bidentate manner in wild-type PhnA, the substrate acetate moiety binds to M1 of the T68A mutant in a monodentate fashion, with one of the oxygen atoms at a distance of 2.5 Å from M1 and the second oxygen pointing away from the metal and hydrogen bonded to a solvent molecule. This water, in turn, is hydrogen bonded to the backbone carbonyl of Ile287 (Figure S1D). The distance of the methylene group of PnA to the M1 metal ion is 2.2 Å, close to the observed distance of 2.4 Å between the M1 ion and the methyl group of bound acetate; the distance to M2 is 4.4 Å. As a consequence of binding of the substrate to both metals, the carbon-carbon-phosphorus bond angle is quite small (102°) with the carbon-phosphorus bond oriented in a way that upon its cleavage would allow electron delocalization into the π system of the metal-bound carboxylate. Hence, it appears that the bound conformation of PnA to the T68A mutant resembles the productive complex for catalysis.

The suggested mode of monodentate stabilization of an enolate intermediate by a metal ion is reminiscent of mandelate racemase enzymes (Gerlt et al., 2005). Mechanistic and crystallographic studies of this enzyme have demonstrated that an enolate intermediate of mandelate is stabilized by a divalent magnesium ion that binds only one of the oxygen atoms of the intermediate. This oxygen also interacts with a Lys. The second oxygen atom of the enolate of mandelate is coordinated by a strictly conserved glutamate side chain (Kallarakal et al., 1995), and the enolate anion is further stabilized by resonance with an aromatic ring. In PhnA, only a water is hydrogen bonded to the second oxygen of the carboxylate.

Crystal Structure of Phosphonoformate-Bound PhnA

Kinetic analyses in this and previous studies (Kim et al., 2011; McGrath et al., 1995) have identified PnF as an inhibitor of PnA hydrolase. We determined competitive inhibition of PhnA by PnF with a K_I value of 33 ± 7 μM (see Supplemental Information and Figure S3). McGrath et al. (1995) hypothesized that the inhibition of PnA hydrolase from *P. fluorescens* 23F could be due to the similar structures of PnA and phosphonoformate. In order to delineate the inhibitory mechanism of PnF, we determined the crystal structure of PhnA in the presence of PnF to a resolution of 1.6 Å (Figure 4D). Although no rearrangement of the metal binding side chains was observed, the distance between the zinc ions increased to 4.7 Å.

Compared to the binding of PnA, the phosphonate moiety of PnF is bound to the M1 zinc ion, not the M2 ion. The orientation and position of the PnF is similar to that observed previously in the cocrystal structure of *P. fluorescens* 23F PhnA (Kim et al., 2011). One oxygen atom of the phosphonate is stabilized by electrostatic interactions with the M1 ion positioned 1.85 Å away (Figure 4D). A water-mediated hydrogen-bonding interaction also exists between a second oxygen atom of the phosphonate moiety and the side chain of Asp29. Similarly, the third oxygen atom interacts with the side chain of Asn89 through a water-mediated hydrogen bond. However, the phosphonate is oriented away from the catalytic nucleophile Thr68 (3.4 Å), and the formate is oriented toward this residue, resulting in the inhibitor binding in a backward fashion. The angle defined by the oxygen atom of the Thr68 side chain and the C-P bond is 71°, suggesting that inhibitor binding does not mimic substrate binding. Given the predicted geometry for the transition state of P-O bond formation and P-C bond cleavage, PnF appears to bind in a nonproductive manner through various stabilizing interactions. The carboxylate group is positioned toward the sites of the vanadate equatorial oxygen atoms. One of the carboxylate oxygen atoms is 3.0 Å away from the backbone amide of Thr68 and is involved in a hydrogen-bonding interaction, and the other oxygen atom interacts with a water molecule, which in turn is hydrogen-bonded to the side chain of Asn89 and backbone amide of Asn69. Hence, according to the PnA cocrystal structure and vanadate covalent complex structure, inhibition of enzymatic activity by PnF does not seem to be dependent upon an analogous binding mode of the substrate and inhibitor molecules, but rather upon the tight but nonproductive binding interactions of this molecule in the active site of the enzyme.

DISCUSSION

Currently, four phosphonate catabolic pathways involving cleavage of the C-P bond are known. Apart from the poorly characterized and highly promiscuous C-P lyase pathway, the C-P bond-cleaving enzymes in the other three pathways require the presence of a carbonyl moiety in the β-position to the phosphorus atom. However, the utilization of this β-carbonyl moiety by the three enzymatic mechanisms is vastly different. The PnAA hydrolyzing enzyme uses this group to generate a Schiff-base intermediate that activates the phosphonate group for attack by an active site nucleophile and provides resonance stabilization for the developing negative charge on carbon (Morais et al., 2000). PnPy hydrolase utilizes the β-carbonyl group for stabilization of the pyruvate leaving group by delocalizing the developing negative charge on the methylene group to the carbonyl oxygen (Chen et al., 2006; Kulakova et al., 2003; Ternan et al., 2000). The mechanism employed by PnA hydrolase, as suggested by the cocrystal structures presented here, also employs charge delocalization onto the β-carbonyl (Figure 5A). The enolate dianion thus formed appears to be further stabilized by coordination to the M1 metal ion, in a mechanism reminiscent of the enolase superfamily enzymes (Gerlt et al., 2005). In most members of the enolase superfamily, the metal (Mg^{2+}) binds to both oxygens of the carboxylate of the substrate that will carry the majority of the charge upon enolate formation. Only for mandelate racemase and related enzymes is bidentate binding not observed, and only one of the carboxylate oxygens is coordinated to a Mg^{2+} ion, similar to the observations in this study for PhnA.

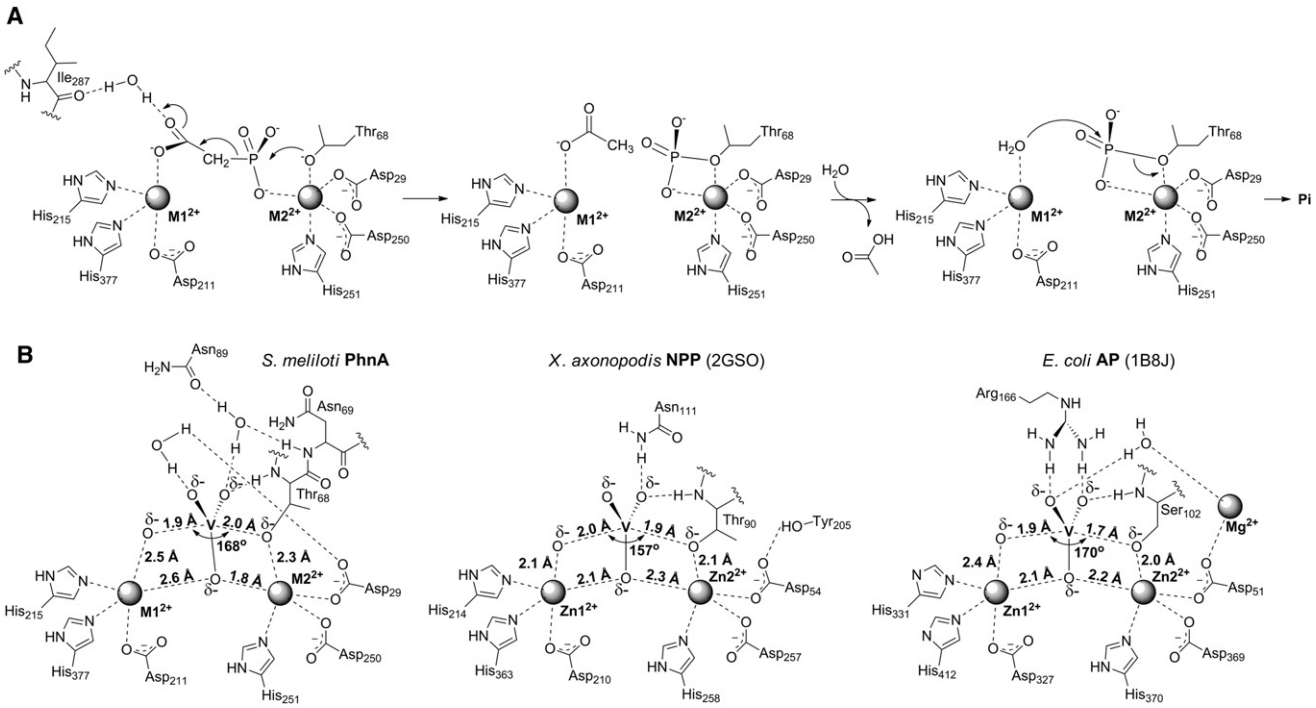

Figure 5. Putative Mechanism for PnA Hydrolysis by PhnA

(A) Proposed mechanism for PhnA.

(B) Scheme of *S. meliloti* PhnA active site structure with vanadate bound used as transition state model as compared to AP (PDB Code: 1B8J) (Holtz et al., 1999) and NPP (PDB Code: 2GSO) (Zalatan et al., 2006).

From our data, the stabilization of developing negative charge on the leaving group by the M1 metal ion appears to be a conserved feature of the alkaline phosphatase superfamily members, albeit the manner by which the active site geometry is used differs considerably from phosphate ester hydrolysis. Compared to AP and NPP, PhnA must activate a much weaker, carbon-based leaving group instead of an oxygen-based leaving group. As a measure of leaving group ability, the pK_a of the conjugate acid of the acetate enolate is likely to be >30 (Richard and Amyes, 2001) compared to a typical alcohol pK_a of ~15–18. In addition to the different leaving group ability, the charge distribution on the leaving group is also significantly different. During phosphate ester hydrolysis, significant charge build-up occurs on the bridging oxygen of the leaving group, and this charge is stabilized by the M1 ion (O'Brien and Herschlag, 2002; Zalatan et al., 2007). For phosphonate hydrolysis, the charge is delocalized such that most of the charge likely resides on the oxygens of the acetate enolate (Figure 5A). This charge would be situated further from the oxygen of the Thr nucleophile coordinated to the M2 ion as compared to AP and NPP. Thus, a longer metal-metal distance appears to be required to simultaneously stabilize the developing charge on the leaving group with the M1 ion and activate the Thr nucleophile with the M2 ion. The involvement of Thr68 as a nucleophile is supported by a recent study on PhnA from *P. fluorescens* (Kim et al., 2011) that reported loss of activity when the corresponding residue was mutated and that demonstrated labeling of the Thr hydroxyl with a phosphate group when incubated with $\gamma-^{32}$P-ATP, a slow substrate for PhnA. Thus, only the relatively long Zn-Zn distance allows the PnA substrate to simultaneously bind to both metals in a conformation that supports formation of an acetate enolate intermediate.

How PhnA can stabilize the much weaker leaving group with essentially the same active site architecture as that of AP and NPP to achieve effective catalysis is at present not clear. Unlike the extensive studies of enzymatic and nonenzymatic hydrolysis of phosphate monoesters and phosphate diesters, which have provided a detailed picture of transition state structures, very little is known about the transition state structure for C-P bond cleavage. Although at present it is not clear which features of the active site geometry of PhnA facilitate efficient catalysis beyond electrostatic stabilization of the leaving group, a plausible explanation can be offered for the previously reported poor activity for phosphate ester hydrolysis (Kim et al., 2011). AP has been shown to utilize strong electrostatic stabilization of the negative charge of the nonbridging oxygens by the binuclear Zn^{2+} cluster (Nikolic-Hughes et al., 2005). On the basis of structures of AP with vanadate bound (PDB Code: 1B8J) (Holtz et al., 1999), one of the nonbridging oxygens is believed to interact with both metals in the transition state (Figure 5B). On the other hand, the vanadate structure of PhnA is decidedly nonsymmetric, with the corresponding equatorial oxygen interacting much more strongly with M2 than with M1.

The formation of a stabilized acetate enolate dianion was also recently proposed for PnA hydrolysis by *P. fluorescens* PhnA on the basis of structural and mechanistic studies (Kim et al., 2011). In that study, stabilization of the enolate oxygens was proposed to be achieved by interactions with two conserved lysine

residues (Lys126 and Lys128), rather than through stabilization by the M1 metal. This mechanistic proposal was based on modeling of the substrate according to the cocrystal structure of *P. fluorescens* PhnA with PnF. These two lysine residues are also conserved in *S. meliloti* PhnA (Lys130 and Lys132). However, in our structures, these residues are far away from the ligands and are not involved in any binding interactions with these ligands. In order to test the importance of these residues in *S. meliloti* PhnA, we generated single Ala mutations at Lys130 and Lys132 and monitored the activity of these variants. Consistent with the observations with *P. fluorescens* PhnA (Kim et al., 2011), mutation at either of these lysines in *S. meliloti* PhnA resulted in inactive enzyme (Table S1). The loss of activity need not imply a direct role of these residues in enolate stabilization and may also be due to secondary effects, such as detrimental changes in the solvent structure in the active site, as observed for the N89V mutant. Although we cannot at present rule out that these Lys residues do play a role in stabilization of the leaving group, we favor the model in Figure 5A for the following reasons. First, our mechanistic proposal for the role of the M1 metal in stabilizing the enolate oxygen is based on direct crystallographic observation of substrate PnA bound to the T68A mutant. Second, the orientation of PnA bound to the T68A mutant is consistent with the geometric constraints of a predicted in-line displacement reaction whereas the orientation of PnF is not. The active sites of *S. meliloti* and *P. fluorescens* enzymes are very similar, but a few differences exist between the two enzymes, most notably the recombinant enzyme from *S. meliloti*, as isolated from *E. coli*, is monomeric, whereas the enzyme from *P. fluorescens* is a dimer (Kim et al., 2011). Detailed mechanistic studies will be required to distinguish between the two strategies of enolate stabilization that have been proposed on the basis of the available structural information.

SIGNIFICANCE

Bacteria have evolved the ability to metabolize phosphonates as a nutrient source for phosphorus, using chemistry that results in the cleavage of the inert C-P bond. The structural and biochemical studies presented here provide insights into the mechanism of C-P bond cleavage by *S. meliloti* PhnA, which represents a poorly studied activity within the catalytic repertoire of the alkaline phosphatase superfamily. We show that PhnA bears an atypically spaced bimetallic center and that this larger intermetal distance may be utilized to accommodate the distance between the entering nucleophile and the charge-bearing atoms of the leaving group in the transition state during C-P bond cleavage.

EXPERIMENTAL PROCEDURES

Materials, Culture Conditions, and DNA Manipulations

Chemicals were obtained from Sigma-Aldrich (St. Louis, MO) or Thermo Fisher Scientific (Pittsburgh, PA) and were used without further purification. The purity of the commercially obtained PnA (Sigma-Aldrich) was verified by ^{1}H NMR analysis and showed no acetate contamination (detection limit was less than 0.014 molar percentage). Media components were purchased from Thermo Fisher Scientific or VWR (West Chester, PA). The strains and plasmids used in this study are listed in Table S2. Details of culture conditions and DNA manipulations are described in Supplemental Information.

Cloning, Protein Expression, Purification, and Crystallization

Cloning, expression, and purification of recombinant *S. meliloti* PhnA from *E. coli* has been described previously (Borisova et al., 2011). For crystallization, the hexahistidine tag was removed by digestion with thrombin (1 unit/mg of protein) followed by purification using anion exchange (5 ml of HiTrap Q-FF, GE Healthcare) and size exclusion chromatographies (Superdex 75 16/60, GE Healthcare). The purified recombinant protein was a monomer in solution, as determined using analytical size exclusion chromatography. Apo protein at a final concentration of 20 mg/mL in 20 mM HEPES and 100 mM KCl (pH 7.5) buffer was used for sparse matrix crystallization screening trials, using the hanging drop vapor diffusion technique. Diffraction quality crystals were obtained in two mother liquor conditions at 9°C: 25% PEG 3350, 0.2 M sodium chloride, and 0.1 M Tris (pH 8.5), and 25% PEG 3350, 0.2 M ammonium acetate, and 0.1 M HEPES (pH 7.5). Crystals typically took three days to grow and were briefly soaked in mother liquor supplemented with 15% glycerol prior to vitrification in liquid nitrogen. PhnA mutants were generated using standard procedures for site-directed mutagenesis and were expressed, purified, and crystallized according to the protocols for wild-type enzyme. The purity of all protein samples was greater than 95%, as judged by SDS-polyacrylamide gel electrophoresis.

The PhnA mutant T68A was incubated with 2 mM zinc chloride and 10 mM PnA for 2 hr on ice prior to sparse screening for crystallization. Cocrystals of PhnA T68A mutant in complex with PnA were obtained in the crystallization condition 20% PEG 3350 and 0.2 M ammonium chloride and were briefly soaked in cryoprotectant solution of mother liquor supplemented with 20% glycerol, 5 mM zinc chloride, and 50 mM PnA prior to vitrification in liquid nitrogen. Cocrystals of the complex with PnF were obtained by soaking apo protein crystals in 10 mM of PnF in the mother liquor for 12 hr. Metal ions were soaked by supplementing the mother liquor with 5 mM of zinc chloride, 5 mM manganese chloride, or 5 mM of iron(II) ammonium sulfate for 3 hr. To generate the covalently bound vanadate complex, apo protein was incubated on ice for 10 min with 2 mM freshly boiled sodium orthovanadate solution and then was crystallized in the manner described above.

PhnA Enzyme Kinetics

The formation of inorganic phosphate from PnA by the action of N-terminally hexahistidine-tagged PhnA (PhnA-N-His) was detected by a discontinuous assay using a Malachite Green phosphate assay kit (BioAssay Systems, Hayward, CA). Assay mixtures (500 μl total volume) containing 50 mM HEPES-K (pH 7.5) and 0.42 μM PhnA-N-His were preincubated at 30°C for 8 min, and the reaction was initiated by the addition of PnA stock solutions to final concentrations of 0–400 μM. Aliquots of the reaction mixture (80 μl) were taken out every 20 s over a period of 2 min, quenched by addition to 20 μl of Malachite Green reagent prepared as per the manufacturer's instruction, and incubated at room temperature for 30 min for color development. The assays were done in duplicate. The absorbance at 620 nm was plotted against the reaction time, and the rate of A_{620} increase was converted to the rate of phosphate formation using a linear calibration curve prepared with known concentrations of inorganic phosphate standard (0–40 μM). The initial rates of phosphate formation were fit to the Michaelis-Menten equation ($V_0 = ([S] * V_{max}) / ([S] + K_M)$) using the IGOR Pro 6.1 software package (WaveMetrics, Portland, OR) in order to determine steady state kinetic parameters of PhnA-N-His. The kinetics data are summarized in Table 2 and Figure S2.

To evaluate the divalent metal dependence of PhnA-N-His, 10 μM $ZnCl_2$, $MgCl_2 \times 6H_2O$, $MnCl_2 \times 4H_2O$, $CoCl_2 \times 6H_2O$, or $(NH_4)_2Fe(SO_4)_2 \times 6H_2O$ were added to the assay mixture prior to the preincubation period, and assays were performed as described above. The concentrations of PhnA-N-His were adjusted (0.07–0.48 μM) to allow for the detection of product formation within the linear range of the assay. Assays in the presence of oxygen-sensitive Fe(II) were set up in an anaerobic chamber obtained from Coy Laboratory Products, Inc. (Grass Lake, MI) under an atmosphere of N_2 and H_2 (95%/5%). The aliquots of buffer-enzyme solution containing Fe(II) were subsequently brought outside the glove box in tightly capped eppendorf tubes, followed by preincubation and reaction initiation with PnA as described above. The kinetics data are summarized in Table 2 and Figure S2.

Metal-free PhnA-N-His was prepared by treatment of the protein with 8.3 mM EDTA sodium salt at 4°C for 3 hr with gentle agitation followed by size exclusion chromatography using a PD-10 desalting column (GE

Healthcare, Piscataway, NY) eluted with 50 mM HEPES-K, 0.2 M NaCl, and 10% glycerol (pH 7.5). Following EDTA treatment, less than 0.02 Zn^{2+} ions per PhnA monomer were detected indicating nearly complete removal by EDTA treatment. The resulting apo PhnA-N-His was tested in the activity assay as described above with and without addition of Zn^{2+}, Mn^{2+}, or Fe^{2+} (Table 2; Figure S2). When combinations of two divalent metal cations were studied (at 10 μM each) initial rates of product formation were measured at 200 μM PnA (Table S1, left).

PhnA exchanged into Chelex-treated buffer via a series of dilution-concentration steps to remove excess metal ions contained only 0.5 Zn^{2+} ions per monomer, as determined using PAR assay (Hunt et al., 1984; Okeley et al., 2003). Because of the partial dissociation of the bound metal ions from PhnA during attempts to separate the protein from the constituents of the reconstitution buffer, the identity of the PhnA-bound metal ion(s) in PhnA reconstituted with different metals could not be characterized directly.

Enzymatic activity of PhnA mutants purified as described above but not treated with EDTA (at 10 μM, except for the T68A mutant at 5 μM) was measured as described above in the presence of 20 μM Mn^{2+} and 0.2 or 1.0 mM PnA (Table S1, right). The formation of Pi was monitored over a period of 0.5–1 hr.

Phasing and Structure Determination

A ten-fold redundant data set was collected from crystals of *S. meliloti* PhnA to a limiting resolution of 1.35 Å (overall R_{merge} = 0.068, I/σ(I) = 1.8 in the highest resolution shell) utilizing a Mar 300 CCD detector (LS-CAT, Sector 21 ID-D, Advanced Photon Source, Argonne, IL). The structure of PhnA was solved by single wavelength anomalous diffraction utilizing anomalous scattering from a mercury derivative (6-fold redundancy with R_{merge} = 0.084, I/σ(I) = 3.2 in the highest resolution shell). Data were indexed and scaled using the HKL-2000 package (Otwinowski et al., 2003). Mercury sites were identified using HySS, and the heavy atom substructure was imported to SHARP for maximum likelihood refinement and phase calculation, yielding an initial figure of merit of 0.497 to 1.9 Å resolution. Solvent flattening using DM further improved the quality of the initial map, and most of the main chain could be built using ARP/wARP (Perrakis et al., 1997). Cross-validation used 5% of the data in the calculation of the free R factor (Kleywegt and Brünger, 1996). The remainder of the model was fitted using XtalView and further improved by rounds of refinement with REFMAC (Murshudov et al., 1997; Murshudov et al., 1999) interspersed with rounds of manual building using XtalView (McRee, 1999).

The cocrystal structures of PhnA with PnA, acetate, phosphonoformate, and vanadate were determined, to resolutions of 2.1 Å, 2.0 Å, 1.6 Å, and 1.8 Å, respectively, by molecular replacement using the coordinates of native PhnA as a search probe. Each of the structures was refined and validated using the procedures detailed above. Cross-validation was routinely used throughout the course of model building and refinement using 5% of the data in the calculation of the free R factor. For each of the structures, the stereochemistry of the model was monitored throughout the course of refinement using PROCHECK (Laskowski et al., 1996). Relevant data collection and refinement statistics are provided in Table 1.

ACCESSION NUMBERS

Coordinates have been deposited in the Protein Data Bank (http://www.rcsb.org) with the following accession codes: PhnA (native) (3SZY), PhnA-Vanadate (3T00), T68A PhnA-PnA (3T02), PhnA-Acetate (3SZZ), and PhnA-PnF (3T01).

SUPPLEMENTAL INFORMATION

Supplemental Information includes two tables and three figures and can be found with this article online at doi:10.1016/j.chembiol.2011.07.019

ACKNOWLEDGMENTS

This work was supported by the National Institutes of Health (grant GM PO1 GM077596) and the Howard Hughes Medical Institute. Its contents are solely the responsibility of the authors and do not necessarily represent the official views of the National Institute of General Medical Sciences, National Institutes of Health, or Howard Hughes Medical Institute. The authors thank Drs. Keith Brister, Spencer Anderson, and Joseph Brunzelle at LS-CAT (23-ID at Argonne National Laboratories, APS) for facilitating crystallographic data collection. The authors thank Prof. John Gerlt for critical reading of this manuscript.

Received: May 18, 2011
Revised: June 24, 2011
Accepted: July 15, 2011
Published: October 27, 2011

REFERENCES

Borisova, S.A., Christman, H.D., Metcalf, M.E., Zulkepli, N.A., Zhang, J.K., van der Donk, W.A., and Metcalf, W.W. (2011). Genetic and biochemical characterization of a pathway for the degradation of 2-aminoethylphosphonate in *Sinorhizobium meliloti* 1021. J. Biol. Chem. *286*, 22283–22290.

Chen, C.C., Han, Y., Niu, W., Kulakova, A.N., Howard, A., Quinn, J.P., Dunaway-Mariano, D., and Herzberg, O. (2006). Structure and kinetics of phosphonopyruvate hydrolase from *Variovorax* sp. Pal2: new insight into the divergence of catalysis within the PEP mutase/isocitrate lyase superfamily. Biochemistry *45*, 11491–11504.

Clark, L.L., Ingall, E.D., and Benner, R. (1999). Marine organic phosphorus cycling: novel insights from nuclear magnetic resonance. Am. J. Sci. *299*, 724–737.

Coleman, J.E. (1992). Structure and mechanism of alkaline phosphatase. Annu. Rev. Biophys. Biomol. Struct. *21*, 441–483.

Forlani, G., Klimek-Ochab, M., Jaworski, J., Lejczak, B., and Picco, A.M. (2006). Phosphonoacetic acid utilization by fungal isolates: occurrence and properties of a phosphonoacetate hydrolase in some penicillia. Mycol. Res. *110*, 1455–1463.

Galperin, M.Y., Bairoch, A., and Koonin, E.V. (1998). A superfamily of metalloenzymes unifies phosphopentomutase and cofactor-independent phosphoglycerate mutase with alkaline phosphatases and sulfatases. Protein Sci. *7*, 1829–1835.

Gerlt, J.A., Babbitt, P.C., and Rayment, I. (2005). Divergent evolution in the enolase superfamily: the interplay of mechanism and specificity. Arch. Biochem. Biophys. *433*, 59–70.

Holtz, K.M., Stec, B., and Kantrowitz, E.R. (1999). A model of the transition state in the alkaline phosphatase reaction. J. Biol. Chem. *274*, 8351–8354.

Hunt, J.B., Neece, S.H., Schachman, H.K., and Ginsburg, A. (1984). Mercurial-promoted Zn^{2+} release from *Escherichia coli* aspartate transcarbamoylase. J. Biol. Chem. *259*, 14793–14803.

Kallarakal, A.T., Mitra, B., Kozarich, J.W., Gerlt, J.A., Clifton, J.G., Petsko, G.A., and Kenyon, G.L. (1995). Mechanism of the reaction catalyzed by mandelate racemase: structure and mechanistic properties of the K166R mutant. Biochemistry *34*, 2788–2797.

Kim, A., Benning, M.M., OkLee, S., Quinn, J., Martin, B.M., Holden, H.M., and Dunaway-Mariano, D. (2011). Divergence of chemical function in the alkaline phosphatase superfamily: structure and mechanism of the P-C bond cleaving enzyme phosphonoacetate hydrolase. Biochemistry *50*, 3481–3494.

Kim, E.E., and Wyckoff, H.W. (1991). Reaction mechanism of alkaline phosphatase based on crystal structures. Two-metal ion catalysis. J. Mol. Biol. *218*, 449–464.

Kleywegt, G.J., and Brünger, A.T. (1996). Checking your imagination: applications of the free R value. Structure *4*, 897–904.

Kononova, S.V., and Nesmeyanova, M.A. (2002). Phosphonates and their degradation by microorganisms. Biochemistry (Mosc.) *67*, 184–195.

Kulakova, A.N., Kulakov, L.A., and Quinn, J.P. (1997). Cloning of the phosphonoacetate hydrolase gene from *Pseudomonas fluorescens* 23F encoding a new type of carbon-phosphorus bond cleaving enzyme and its expression in *Escherichia coli* and *Pseudomonas putida*. Gene *195*, 49–53.

Kulakova, A.N., Wisdom, G.B., Kulakov, L.A., and Quinn, J.P. (2003). The purification and characterization of phosphonopyruvate hydrolase, a novel

carbon-phosphorus bond cleavage enzyme from *Variovorax* sp Pal2. J. Biol. Chem. *278*, 23426–23431.

Laskowski, R.A., Rullmannn, J.A., MacArthur, M.W., Kaptein, R., and Thornton, J.M. (1996). AQUA and PROCHECK-NMR: programs for checking the quality of protein structures solved by NMR. J. Biomol. NMR *8*, 477–486.

Lassila, J.K., and Herschlag, D. (2008). Promiscuous sulfatase activity and thio-effects in a phosphodiesterase of the alkaline phosphatase superfamily. Biochemistry *47*, 12853–12859.

McGrath, J.W., Wisdom, G.B., McMullan, G., Larkin, M.J., and Quinn, J.P. (1995). The purification and properties of phosphonoacetate hydrolase, a novel carbon-phosphorus bond-cleavage enzyme from *Pseudomonas fluorescens* 23F. Eur. J. Biochem. *234*, 225–230.

McMullan, G., Harrington, F., and Quinn, J.P. (1992). Metabolism of phosphonoacetate as the sole carbon and phosphorus source by an environmental bacterial isolate. Appl. Environ. Microbiol. *58*, 1364–1366.

McRee, D.E. (1999). XtalView/Xfit: a versatile program for manipulating atomic coordinates and electron density. J. Struct. Biol. *125*, 156–165.

Metcalf, W.W., and van der Donk, W.A. (2009). Biosynthesis of phosphonic and phosphinic acid natural products. Annu. Rev. Biochem. *78*, 65–94.

Morais, M.C., Zhang, W., Baker, A.S., Zhang, G., Dunaway-Mariano, D., and Allen, K.N. (2000). The crystal structure of *Bacillus cereus* phosphonoacetaldehyde hydrolase: insight into catalysis of phosphorus bond cleavage and catalytic diversification within the HAD enzyme superfamily. Biochemistry *39*, 10385–10396.

Murshudov, G.N., Vagin, A.A., and Dodson, E.J. (1997). Refinement of macromolecular structures by the maximum-likelihood method. Acta. Crystallogr. D Biol. Crystallogr. *53*, 240–255.

Murshudov, G.N., Vagin, A.A., Lebedev, A., Wilson, K.S., and Dodson, E.J. (1999). Efficient anisotropic refinement of macromolecular structures using FFT. Acta. Crystallogr. D Biol. Crystallogr. *55*, 247–255.

Nikolic-Hughes, I., O'Brien, P.J., and Herschlag, D. (2005). Alkaline phosphatase catalysis is ultrasensitive to charge sequestered between the active site zinc ions. J. Am. Chem. Soc. *127*, 9314–9315.

O'Brien, P.J., and Herschlag, D. (2002). Alkaline phosphatase revisited: hydrolysis of alkyl phosphates. Biochemistry *41*, 3207–3225.

Okeley, N.M., Paul, M., Stasser, J.P., Blackburn, N., and van der Donk, W.A. (2003). SpaC and NisC, the cyclases involved in subtilin and nisin biosynthesis, are zinc proteins. Biochemistry *42*, 13613–13624.

Otwinowski, Z., Borek, D., Majewski, W., and Minor, W. (2003). Multiparametric scaling of diffraction intensities. Acta Crystallogr. A *59*, 228–234.

Panas, P., Ternan, N.G., Dooley, J.S., and McMullan, G. (2006). Detection of phosphonoacetate degradation and phnA genes in soil bacteria from distinct geographical origins suggest its possible biogenic origin. Environ. Microbiol. *8*, 939–945.

Perrakis, A., Sixma, T.K., Wilson, K.S., and Lamzin, V.S. (1997). wARP: improvement and extension of crystallographic phases by weighted averaging of multiple-refined dummy atomic models. Acta Crystallogr. D Biol. Crystallogr. *53*, 448–455.

Quinn, J.P., Kulakova, A.N., Cooley, N.A., and McGrath, J.W. (2007). New ways to break an old bond: the bacterial carbon-phosphorus hydrolases and their role in biogeochemical phosphorus cycling. Environ. Microbiol. *9*, 2392–2400.

Richard, J.P., and Amyes, T.L. (2001). Proton transfer at carbon. Curr. Opin. Chem. Biol. *5*, 626–633.

Schwartz, J.H., and Lipmann, F. (1961). Phosphate incorporation into alkaline phosphatase of *E. coli*. Proc. Natl. Acad. Sci. U S A *47*, 1996–2005.

Stec, B., Holtz, K.M., and Kantrowitz, E.R. (2000). A revised mechanism for the alkaline phosphatase reaction involving three metal ions. J. Mol. Biol. *299*, 1303–1311.

Ternan, N.G., Hamilton, J.T., and Quinn, J.P. (2000). Initial in vitro characterisation of phosphonopyruvate hydrolase, a novel phosphate starvation-independent, carbon-phosphorus bond cleavage enzyme in *Burkholderia cepacia* Pal6. Arch. Microbiol. *173*, 35–41.

Thomas, S., Burdett, H., Temperton, B., Wick, R., Snelling, D., McGrath, J.W., Quinn, J.P., Munn, C., and Gilbert, J.A. (2010). Evidence for phosphonate usage in the coral holobiont. ISME J. *4*, 459–461.

Wackett, L.P., Shames, S.L., Venditti, C.P., and Walsh, C.T. (1987). Bacterial carbon-phosphorus lyase: products, rates, and regulation of phosphonic and phosphinic acid metabolism. J. Bacteriol. *169*, 710–717.

Wang, J., Stieglitz, K.A., and Kantrowitz, E.R. (2005). Metal specificity is correlated with two crucial active site residues in *Escherichia coli* alkaline phosphatase. Biochemistry *44*, 8378–8386.

White, A.K., and Metcalf, W.W. (2007). Microbial metabolism of reduced phosphorus compounds. Annu. Rev. Microbiol. *61*, 379–400.

Wojciechowski, C.L., Cardia, J.P., and Kantrowitz, E.R. (2002). Alkaline phosphatase from the hyperthermophilic bacterium *T. maritima* requires cobalt for activity. Protein Sci. *11*, 903–911.

Wojciechowski, C.L., and Kantrowitz, E.R. (2002). Altering of the metal specificity of *Escherichia coli* alkaline phosphatase. J. Biol. Chem. *277*, 50476–50481.

Zalatan, J.G., Catrina, I., Mitchell, R., Grzyska, P.K., O'Brien, P.J., Herschlag, D., and Hengge, A.C. (2007). Kinetic isotope effects for alkaline phosphatase reactions: implications for the role of active-site metal ions in catalysis. J. Am. Chem. Soc. *129*, 9789–9798.

Zalatan, J.G., Fenn, T.D., Brunger, A.T., and Herschlag, D. (2006). Structural and functional comparisons of nucleotide pyrophosphatase/phosphodiesterase and alkaline phosphatase: implications for mechanism and evolution. Biochemistry *45*, 9788–9803.

Zalatan, J.G., Fenn, T.D., and Herschlag, D. (2008). Comparative enzymology in the alkaline phosphatase superfamily to determine the catalytic role of an active-site metal ion. J. Mol. Biol. *384*, 1174–1189.

